Pilot-scale mineralization of flue gas desulfurization gypsum in waste alkali medium

Yuliang Cao[1], Tingfeng Liu[1], Wenyi Tan[1,2], Guodong Chen[1]

[1]Nanjing Institute of Technology, Nanjing, China
[2]Xuzhou University of Technology, Xuzhou, China
Presenting author email: 313198906@qq.com

Abstract

Flue gas desulfurization gypsum (FGDG) mainly comes from the FGD process in thermal power plants, smelters and so on. In this study, FGDG was used as raw material of CO_2 mineralization in NaOH medium in a pilot-scale bubble column reactor. The effects of pH value, CO_2 flow, reaction temperature, liquid level in bubble column reactor on the CO_2 mineralization process were investigated. The obtained crystal, morphology and particle size distribution of mineralization products were also studied. The results show that pH has a significant effect on CO_2 mineralization capacity. CO_2 flow and liquid have a slight effect on the particle size distribution of mineralized products. The crystal, morphology and particle size distribution of the obtained mineralization products were also observed. XRD and SEM show that the FGDG mineralization product is a single clustered crystal. The pilot results provide an optimized evidence for FGDG mineralization.

Keyword： Flue gas desulfurization gypsum (FGDG), NaOH, pilot-scale, mineralization.

1. Introduction

The use of fossil energy emits a large amount of greenhouse gases (CO_2, CH_4, N_2O, O_3, etc.) with the continuous development of global industrialization, which leads to increasing global warming and poses a significant threat to the ecological environment as well as the survival of human beings [1, 2], and thus the reduction of CO_2 emissions is receiving more and more attention [3, 4]. The fundamental way to reduce CO_2 emissions is to use clean energy instead of fossil fuels, however, the large-scale application of clean energy cannot be realized in a short time. Therefore CO_2 storage is a necessary means to achieve CO_2 emission reduction at this stage[5]. Mineral sequestration (mineralization) generates stable products, which can ensure permanent, safe and efficient CO_2 sequestration with sufficiently low risk of leakage, and has been widely focused on by many researchers[6], and this technology performs CO_2 mineralization by precipitating stable carbonate compounds, such as calcium carbonate and magnesium carbonate[7, 8]. Certain natural minerals and industrial solid wastes containing large amounts of Ca^{2+} are used as mineralization feedstock. The environment required for CO_2 mineralization of natural products is harsh and mining, milling and separation make them costly[9]. In contrast, industrial solid wastes such as fly ash [10, 11], waste gypsum [12-14], steel slag [15], and calcium carbide slag [16] have been considered by researchers to have great potential for mineralization due to their relatively high reactivity and easy availability.

FGDG is a by-product of the flue gas wet desulfurization process in coal-fired power plants, and its main component is $CaSO_4 \cdot 2H_2O$, which can be up to 93 wt%. At present, China's annual emissions of desulfurized gypsum are about 80 million tons, with a utilization rate of 78%, and a cumulative stockpile of about 100 million tons[17]. Scholars at home and abroad have conducted a lot of studies on the mineralization of FGDG for CO_2 sequestration. Lee [18] et al. used direct wet mineralization of FGDG to investigate the effects of process parameters such as ammonia concentration, CO_2 flow rate, solid-liquid ratio, and other process parameters on the

conversion rate and CO_2 mineralization efficiency of FGDG. Altiner [14] et al. adopted a "two-step method", that is, NaOH and FGDG were thoroughly mixed to form the $Ca(OH)_2$ suspension, and then CO_2 was introduced into the $Ca(OH)_2$ suspension to form $CaCO_3$ particles, but there were impurities in the product, which affected the purity of the product. Wing [12, 19] et al. proposed an ultrasonic technique to study the effects of different reaction media on the mineralization process and the crystalline shape of the product. Ding [20] studied the process flow of FGDG mineralization of CO_2 in NH_4Cl-H_2O system based on the theory of solubility equilibrium of salt solution and insoluble electrolyte, the carbonation rate can reach 98%, in which the carbonation reaction filtrate can be recycled. Wang [21] proposed a process of amine-promoted carbonation of waste gypsum in conjunction with the regeneration of amine by bipolar membrane electrodialysis (BMED), and seven different types of typical amines were selected as reaction media in the CO_2 mineralization. In spite of inspiring results obtained in terms of carbonation efficiency and CO_2 mineralization capacity, few studies on CO_2 mineralization at pilot scale have been unveiled so far. This paper aims to realize CO_2 mineralization at pilot scale in which FGDG as raw material and NaOH effluent from power plants as reaction medium.

2. Materials and methodology

2.1 Materials

The FGDG used in this study was produced from a thermal power plant in China, the FGDG simple was dried at 105 °C for 8 h to remove surface moisture and sieved to 60 mesh. The purity of $CaSO_4$ in FGDG used in the study is 97%, as determined by wet analysis. X-ray diffraction showed that the main component of the FGDG samples was calcium sulfate dihydrate, as shown in Fig.1. The particle size was measured by using a particle size analyzer (Bettersize 3000 Plus), the average size of the FGDG samples (d_{50}) was 31.18 μm, with 90% of the particles smaller than 83.98 μm. The composition of the sample was analyzed by XRF (ZSX Primuss II, Rigaku), and the FGDG impurities mainly contained SiO_2 and Al_2O_3, as shown in Table 1.

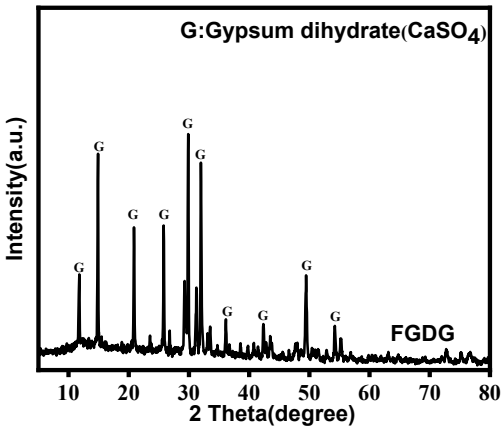

Fig.1 XRD pattern of FGDG.

2.2 CO_2 mineralization experiment

NaOH effluent from power plants pH 8, 10 and 12 were applied for the experiments respectively. The NaOH effluent was pumped into the pilot-scale reactor, as shown in Fig.2. After heating the NaOH effluent to the desired temperature, a weighed FGDG simple was added into the NaOH effluent through the auger, to prepare a slurry, and then 99% CO_2 gas was bubbled into the slurry with vigorous stirring. The effects of reaction temperature (40 °C, 60 °C, 80 °C), pH (8, 10, 12), CO_2 flow rate (20 $L{\cdot}h^{-1}$, 40 $L{\cdot}h^{-1}$, 60 $L{\cdot}h^{-1}$) and liquid level (30 cm, 40 cm, 50 cm) on the FGDG mineralization were investigated. Detailed experimental conditions are shown in Table 2.

For example, pH8-T40-r20-h30 means that the experiments were carried out under the conditions of pH=8, reaction temperature 40 °C, CO_2 flow rate 20 $L{\cdot}h^{-1}$ and liquid level 30 cm. Samples were taken from the exit at a given reaction time for determination (2, 4, 6, 15, 30, and 60 min) and pH was measured at reaction time points (2, 4, 6, 8, 10, 15, 20, 25, 30, 40, 50, and 60 min).

Table 1. Chemical composition of FGDG

Material	CaO	SO_3	SiO_2	Al_2O_3	MgO	Na_2O	K_2O	LOI*
wt%	46.02	46.15	3.6	1.56	0.55	0.17	0.26	1.69

Table 2. Reaction condition in pilot scale experiments

Reaction condition	1	2	3
Temperature, T/°C	40	60	80
pH	8	10	12
CO_2 flow, r/L·h^{-1}	20	40	60
Liquid level, h/cm	30	40	50

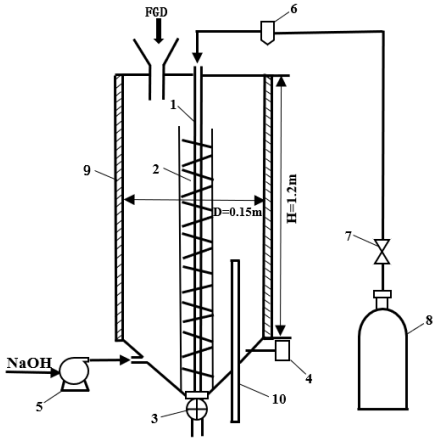

Fig.2 Structure of a pilot-scale mineralization reactor：1- gas tubes，2- heating coils，3-valve，4- pH meter，5- liquid pump，6- gas flow meter，7-gas pressure reducing valves，8- CO_2 cylinders，9- insulation，10- reclaimer tube

2.3 Characterization of product and calculation of storage capacity

All samples were separated from liquid by a high-speed centrifuge, and the obtained solid samples were dried at 180 °C for 8 h. the purity of $CaCO_3$ in the product was calculated from the weight loss of solid samples during the thermogravimetric process under N_2 atmosphere conditions. Pane and Hansen concluded that the decomposition of the $CaCO_3$ occurred at 600 °C to 780 °C[22]. The particle size analyzer (Bettersize3000Plus) was used to determine the particle size distribution of the mineralization products, and the morphology of the products was observed by scanning electron microscopy (SEM). The mass of $CaCO_3$ in the sample at time t is calculated by the following equation:

$$m_{t-CaCO_3} = \frac{\triangle m_{co_2}}{M_{co_2}} \times M_{CaCO_3} \quad (1)$$

$\triangle m_{co_2}$ is the weight of CO_2 that escapes when $CaCO_3$ decomposes during thermogravimetry, m_{t-CaCO_3} is the mass of $CaCO_3$ in the sample of products. M_{CaCO_3} is the relative molecular weight of $CaCO_3$. M_{CO_2} is the relative molecular weight of CO_2. The purity of $CaCO_3$ in the sample at time t is calculated by the following equation:

$$P_{t-CaCO_3} = \frac{m_{t-CaCO_3}}{m_p} \quad (2)$$

Here, P_{t-CaCO_3} is the purity of $CaCO_3$ in the sample of products, m_p is the mass of sample of products.

$$\rho_t = \frac{P_{t-CaCO_3}}{P_{C-CaCO_3}} \quad (3)$$

ρ_t is the CO_2 mineralization efficiency of FGDG, P_{C-CaCO_3} is the purity of $CaCO_3$ when FGDG was 100% mineralized. The purity of $CaSO_4$ in FGDG used in the study is 97%, as determined by wet analysis. Therefore, the purity of the reaction product should be 95.9% for 100% mineralization.

3 Results and Discussion

3.1 Effect of reaction parameters on CO_2 mineralization efficiency

3.1.1 Effect of initial pH on CO_2 mineralization efficiency

The effect of initial pH of NaOH effluent on FGDG mineralization was evaluated by varying initial pH which were 8, 10, 12 (pH8, pH10 and pH12).

Fig.3a shows the variation of slurry pH with time. As CO_2 was introduced into the slurry, the reaction began, and OH^- ions in the slurry was consumed, resulting in a decrease in the pH of the slurry. The pH of the slurry gradually stabilizes to about 7 after about 6 min of continuous reaction. The final pH of the slurry slightly increased with the initial pH of the NaOH effluent increased. The

CO_2 mineralization efficiency of FGDG was also affected by the initial pH of the NaOH effluent. After about 6 min of reaction, the mineralization reaction was basically completed, and then the reaction approached saturation state, as shown in Fig.3b.

The CO_2 mineralization efficiency of FGDG increased slightly with the continuous influx of CO_2 after 6 min of reaction. As the initial pH of NaOH effluent increased from 8 to 12, the CO_2 mineralization efficiency increased from 9.8% to 67.76%. The amount of FGDG involved in the mineralization reaction was small due to the low concentration of OH^- when the pH of the NaOH effluent was respectively 8 and 10. Under all conditions, the CO_2 mineralization efficiency of FGDG and slurry pH tended to stabilize at around 6 min, so this time point was considered the termination point of the basically completed mineralization reaction, as shown in Fig.3a.

The above results indicate that a high pH of NaOH effluent would be beneficial for the mineralization reaction to generate higher purity of $CaCO_3$ in the product, and the mineralization reaction would be more thorough. The high pH of NaOH effluent was ideal for obtaining higher CO_2 mineralization efficiency. The concentration of OH- in the effluent was higher, the leaching Ca^{2+} was more, and the CO_2 mineralization efficiency was higher when the initial pH of NaOH effluent was 12[23, 24].

3.1.2 Effect of CO_2 flow rate on CO_2 mineralization efficiency

The effects of the CO_2 flow rate on CO_2 mineralization was evaluated by varying CO_2 flow rate which were 20, 40 and 60 $L \cdot h^{-1}$ (r20, r40 and r60).

In all cases, the pH of the slurry decreased until it stabilized to 7 at around 6 min, as shown in Fig.4a. The CO_2 mineralization efficiency tended to stabilize when the reaction lasted for about 6 min. However, the final CO_2 mineralization efficiency decreased from 67.76% to 38.35% when the CO_2 flow rate was increased from 20 $L \cdot h^{-1}$ to 60 $L \cdot h^{-1}$, as shown in Fig.4b. Increasing CO_2 flow rate was not conducive to achieving high CO_2 mineralization efficiency of FGDG.

The diameter of the bubble increased and contact area between CO_2 and the slurry decreased with the increased of CO_2 flow rate [25], and the contact time between the CO_2 and the slurry decreases, resulting in the reduction of the mineralization efficiency in reaction products[26], which was not conducive to CO_2 mineralization. However, at 80 °C, the reaction temperature was too high, which reduced the solubility of CO_2 in the liquid, resulting in a decrease in carbonate ion concentration and a decreased in the CO_2 mineralization efficiency [25].

3.1.3 Effect of reaction temperature on the CO_2 mineralization efficiency

The effects of the reaction temperature of the NaOH effluent on the CO_2 mineralization was evaluated by varying the reaction temperature of the NaOH effluent. The CO_2 mineralization

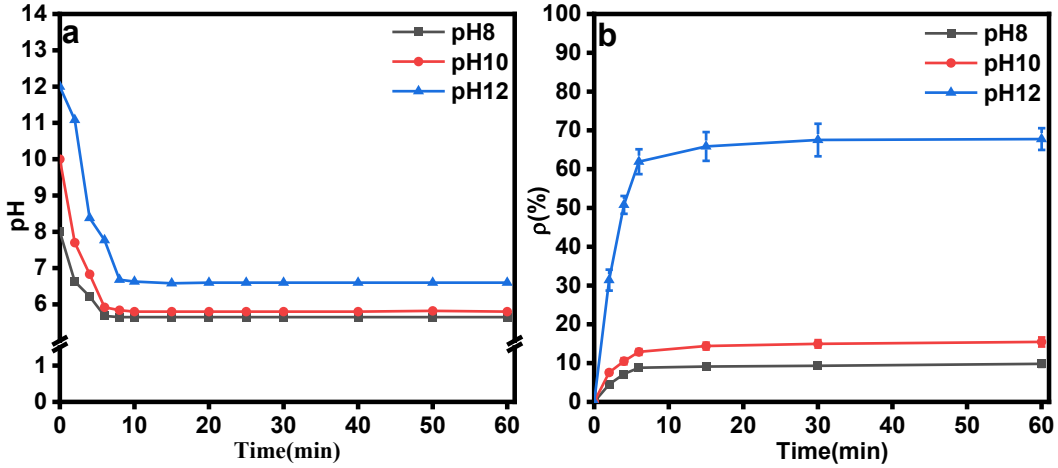

Fig.3 a: The pH value curves depended on time **b**: Effect of initial pH on the mineralization efficiency. (Conditions:40 °C temperature, 20 $L \cdot h^{-1}$ CO_2 flow rate,30 cm liquid level)

efficiency tended to stabilize and the pH of slurry reached 7 after about 6 min when the reaction temperature is 40 °C and 60 °C, as shown in Fig.5a. The time that the CO_2 mineralization efficiency and the pH of slurry to reached stability increased to about 15 min at 80 °C. When the reaction temperature was increased from 40 °C to 60 °C, the CO_2 mineralization efficiency raised from 67.76% to 78.31%. While the reaction temperature was increased from 60 °C to 80 °C, the CO_2 mineralization efficiency was decreased from 75.5% to 55.62%, as shown in Fig.5b. This example demonstrates that increasing the reaction temperature would be beneficial for accelerating the mineralization reaction rate and high CO_2 mineralization efficiency. However, excessive reaction temperature was not conducive to CO_2 mineralization.

From the kinetic point of view, when the temperature was increased from 40 °C to 60 °C, the mass transfer rate could be increased, the thermal motion of the molecule can be promoted and the average kinetic energy of the molecule could be increased, so as to improve the CO_2 mineralization capacity and increased the reaction rate[27].

3.1.4 Effect of liquid level on the CO_2 mineralization efficiency

The effects of the liquid level of the NaOH effluent in the reactor on CO_2 mineralization was evaluated by varying liquid level which were 30, 40 and 50 cm. The difference of liquid level can lead to different capacities of NaOH effluent in the reactor during the experiment. Therefore, it is necessary to change the quantity of FGDG added to ensure that the solid-liquid ratio remains unchanged and the experiment proceeds smoothly. The change of liquid level had no significant

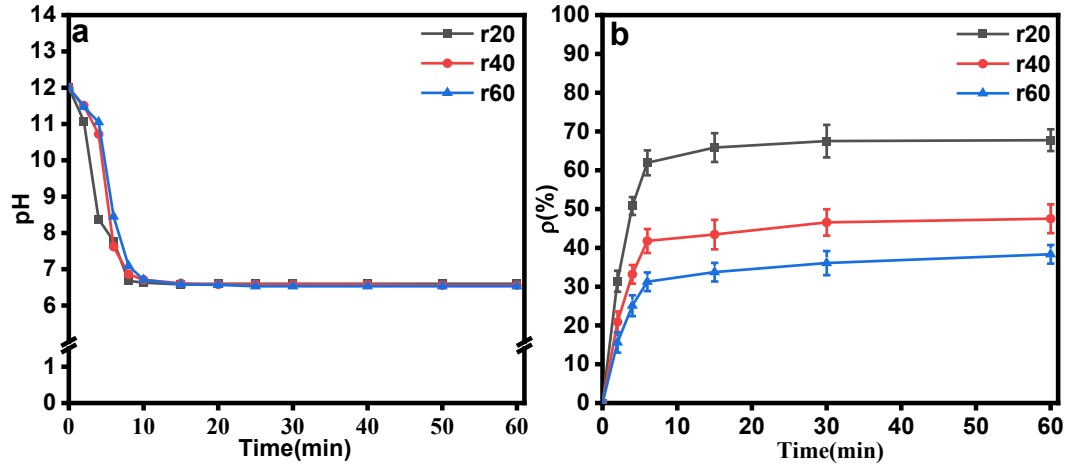

Fig.4 a: The pH value curves depended on time **b**: Effect of CO_2 flow rate on the mineralization efficiency. (Conditions:40°C temperature, pH:12,30 cm liquid level)

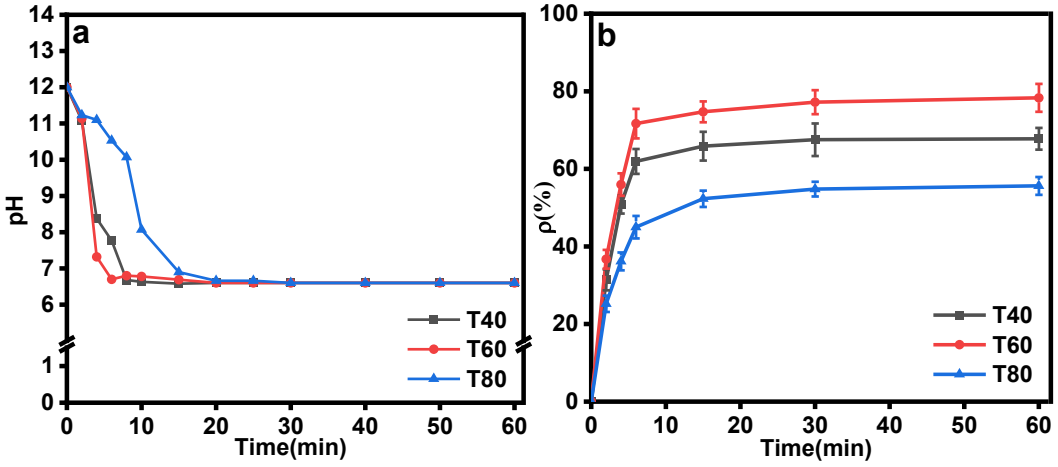

Fig.5 a: The pH value curves depended on time **b**: Effect of reaction temperature on the mineralization efficiency. (Conditions: 20 $L \cdot h^{-1}$ CO_2 flow rate, pH:12, 30 cm liquid level)

process. After about 6 min of reaction, the pH of the slurry decreased to 7, and the decline curve was consistent, as shown in Fig.6a. At the same time, the CO_2 mineralization efficiency tended to stabilize after about 6 min of reaction. When the liquid level increased from 30 to 50 cm, the CO_2 mineralization efficiency increased from 78.31% to 92.15%, as shown in Fig.6b. The above results indicate that a high liquid would be advantageous for high CO_2 mineralization efficiency. However high liquid level could not accelerate CO_2 mineralization reaction rate.

The contact time between the incoming CO_2 and the slurry in the reactor increased with the increased of liquid level, which increased the reaction time of the gas-liquid-solid three-phase in the reactor, thereby promoting the CO_2 mineralization efficiency [28].

3.2 Effect of reaction parameters on product particle size

3.2.1 Effect of initial pH on product particle size

The effect of the initial pH of NaOH effluent on the particle size distribution of the products was investigated by changing the initial pH (pH8, pH10 and pH12). Fig.7 shows the particle size distribution of the product which was generated under different initial pH conditions. The product was in a bimodal particle size distribution and the peaks value were about 2μm and 25μm. When the initial pH were 8, 10 and 12, the d_{50} of the products was 13.4 μm, 11.7 μm and 10.4 μm, respectively. The d_{50} of the products decreased by 29.97% as the initial pH increased from 8 to 12. Therefore, the increased of initial pH would be favorable for obtaining small particle product.

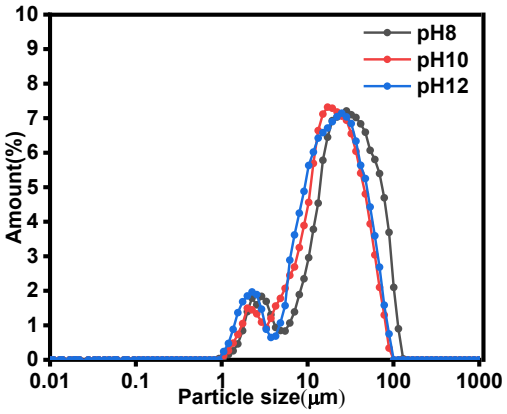

Fig.7 Effect of the pH on particle size distribution of products. (Conditions: 20 L·h^{-1} CO_2 flow rate 40 °C temperature, ,30 cm liquid level)

3.2.2 Effect of CO_2 flow rate on product particle size

The CO_2 flow rate also affected the particle size distribution of the products. Fig.8 shows the influence of CO_2 flow rate on particle size distribution of products. The bimodal peak values of the product were at 1.9 μm and 28.4 μm, and the d_{50} value of product was 10.4 μm at 20 L·h^{-1}. The bimodal peak values of the product were about 3.4 μm and 32.2 μm, then the d_{50} value of products were 17.1 μm and 19.4 μm when the CO_2 flow rate were 40 L·h^{-1} and 60 L·h^{-1}, respectively. The bimodal values of product particle size shifted to the right with the increased

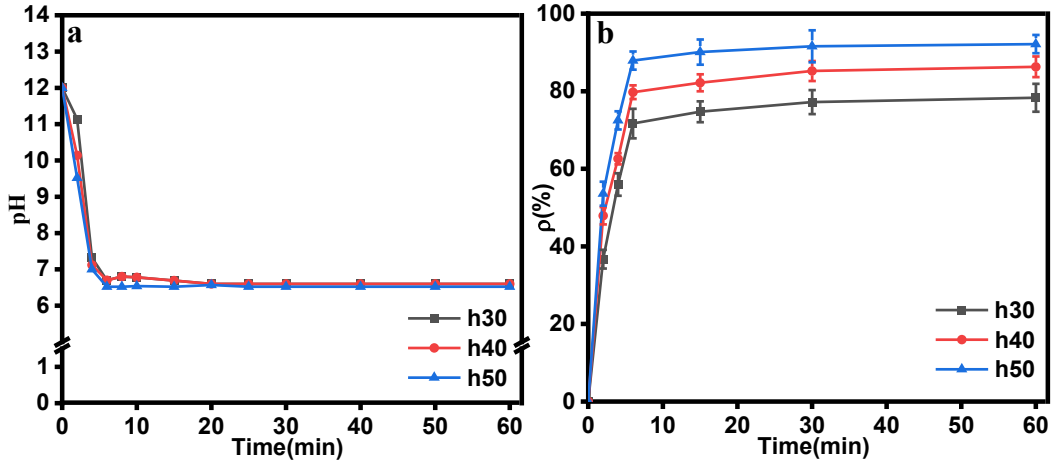

Fig.6 a: The pH value curves depended on time **b**: Effect of liquid level on the mineralization efficiency (Conditions: 20 L·h^{-1} CO_2 flow rate, 60°C temperature, pH:12)

of CO_2 flow rate. The d_{50} of the product decreased by 86.55% as the CO_2 flow rate increased from 20 $L \cdot h^{-1}$ to 60 $L \cdot h^{-1}$. The increased of CO_2 flow rate would be increased the percentage of large particles in the product, which was not conducive to the generation of small particles.

The increased of CO_2 flow rate accelerated crystal growth, so the low CO_2 flow rate was conducive to the acquisition of small particle product. The increased of CO_2 flow rate leaded to more intense churning and stirring of the slurry[29], but at the same time, the drag force of the floating would be greater. Particles with large mass and large particle size was easy to reach high liquid level positions, resulting in large particle size of the product.

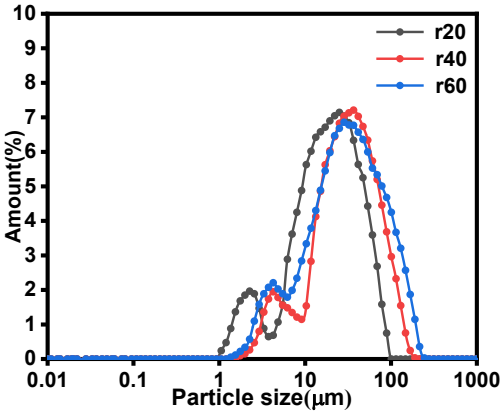

Fig.8 Effect of the CO_2 flow rate on particle size distribution. (Conditions:40°C temperature, pH:12,30 cm liquid level)

3.2.3 Effect of reaction temperature on product particle size

Fig.9 shows that the effect of reaction temperature on particle size distribution in the product. Under all conditions, the product exhibited a bimodal distribution, then the bimodal peak values ranging respectively from 2.3 μm to 2.9 μm and 22.5 μm to 28.4 μm. The d_{50} value of products varied between 10.4 μm to 11.3 μm. The results indicated that the effects of reaction temperature on the particle size distribution of the product was not obvious[30].

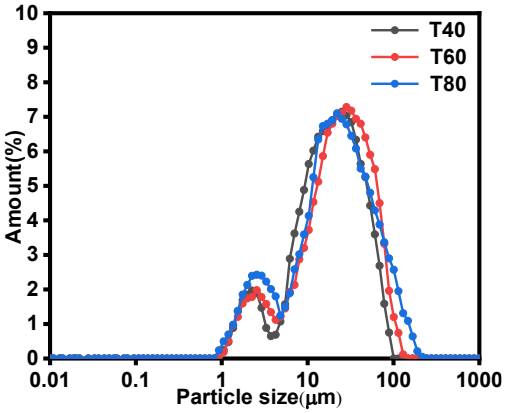

Fig.9 Effect of the reaction temperature on the particle size distribution. (Conditions: 20 $L \cdot h^{-1}$ CO_2 flow rate, pH:12,30 cm liquid level)

3.2.4 Effect of liquid level on product particle size

In this stage, study on the influence of liquid level on product particle size distribution by changing the liquid level inside the reactor. Fig.10 shows a bimodal distribution of product under different conditions of liquid level. The bimodal peak values of the product were at 2.5 μm and 28.4 μm and the d_{50} value of the product was 11.3 μm when the liquid level was 30 cm. The bimodal peak values of the product were at 2.5 μm and 11.7 μm and the d_{50} value of the product was 6.2 μm when the liquid level was 40 cm. The bimodal values of the product were at 1.5 μm and 7.1 μm and the d_{50} value of the product was 4.2 μm when the liquid level was 50 cm. The d_{50} of the product decreased by 62.83% as the increased from 30 cm to 60 cm of liquid level. The corresponding small particle size peaks are more obvious, and the product particle size doublet was shifted to the left with the increase of liquid level.

The above experiments results indicate that a high liquid level would be reduced the percentage of large particles in the product and obtained smaller sized product. The possible reasons for the above phenomenon may be that particles with smaller size is lighter in weight, and under the same drag force, small particle size particles were easy to reach high liquid level positions.

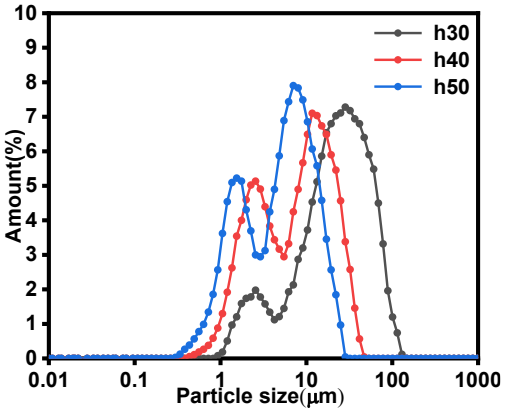

Fig.10 Effect of the liquid level on the particle size distribution. (Conditions:40 °C temperature, pH:12, 20 $L \cdot h^{-1}$ CO_2 flow rate)

3.3 Characterization

3.3.1 Characterization and analysis of product

The main component of dried FGDG was $CaSO_4$ and the main component of the mineralization product was converted into $CaCO_3$ and a small amount of $CaSO_4$ after 60 min of mineralization reaction, as shown in Fig.11. It may be that the FGDG was deposited during the reaction, resulting in the inability of some FGDG to be in full contact with waste NaOH effluent, resulting in insufficient reaction. Fig.12a was a scanning electron microscope (SEM) image of the FGDG. The carbonization products, which was originally diamond-shaped, and the product obtained after carbonization is composed of amorphous nano-sized particles with an aggregate structure[18, 31], as shown in Fig.12b-c. EDS was used to characterize the carbonized products, as shown in Fig.12d, which mainly contained Ca, C and O and were judged to be $CaCO_3$ aggregates.

4 Conclusion

The effects of initial pH of NaOH effluent, CO_2 flow rate, reaction temperature, and liquid level on the mineralization efficiency of FGDG and particle size distribution of products was used to investigate by the FGDG-NaOH carbonization method. The mineralization efficiency of FGDG increased with the increased of initial pH of NaOH effluent, but lower initial pH made it easier to obtain smaller particle products. As the CO_2 flow rate increased from 20 $L \cdot h^{-1}$ to 60 $L \cdot h^{-1}$, the mineralization efficiency of FGDG decreased and the particle size of the product increased. When the reaction temperature was 60 °C, the mineralization efficiency of FGDG was the highest, reaching 92%, and the particle size of the products was almost unaffected by the reaction temperature. High liquid level could be improved the mineralization efficiency of FGDG and also reduced the size of products particles. Through continuous mineralization reactions, rhombic block shaped $CaSO_4$ particles are transformed into aggregates of $CaCO_3$ nanoparticles.

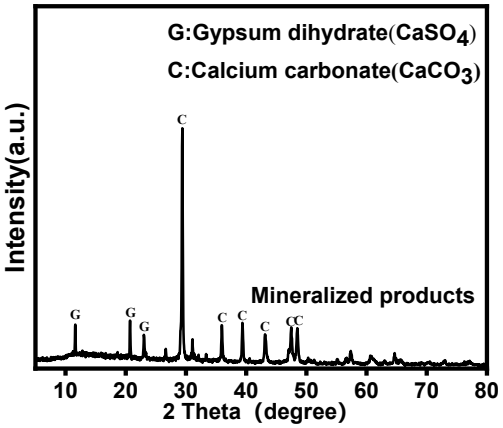

Fig.11 XRD patterns of mineralized products

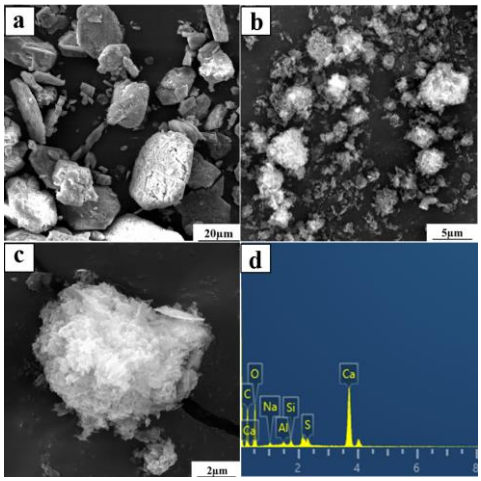

Fig.12 **a**: The SEM images of raw FGDG; **b,-c**: The SEM images of FGDG mineralization product; **d**: EDS mapping of FGDG mineralization product

5 References

1. Dahlke FT, Butzin M, Nahrgang J, Puvanendran V, Mortensen A, Pörtner HO, Storch D (2018): Northern cod species face spawning habitat losses if global warming exceeds 1.5°C. Science advances 4, eaas8821
2. Zhu C, Kobayashi K, Loladze I, Zhu J, Jiang Q, Xu X, Liu G, Seneweera S, Ebi KL, Drewnowski A, Fukagawa NK, Ziska LH Carbon dioxide (CO_2) levels this century will alter the protein, micronutrients, and vitamin content of rice grains with potential health consequences for the poorest rice-dependent countries. Science advances 4, eaaq1012
3. Schwartz SEJAJoP (2018): Resource Letter GECC-2: The Greenhouse Effect and Climate Change: The Intensified Greenhouse Effect
4. Longgui X, Liping M, Wei Z, (2022): Research progress of carbon sequestration technology of industrial solid waste gypsum. Phosphate & Compound Fertilizer 37, 32-35
5. Jiang K, Ashworth P (2021): The development of Carbon Capture Utilization and Storage (CCUS) research in China: A bibliometric perspective. Renewable and Sustainable Energy Reviews 138, 110521
6. Seifritz W (1990): CO_2 disposal by means of silicates. Nature 345, 486-486
7. Jingwei R, Tao W, Yulei C, Yan W, Yunxi D, Shenmeng D, Jinzhi D(2020): Research status and application potential of CO_2 mineralization. Earth Science 45, 2413-2425
8. Pandey S, Srivastava V, Kumar V (2020): Comparative thermodynamic analysis of CO_2 based dimethyl carbonate synthesis routes. The Canadian Journal of Chemical Engineering 99
9. Pan S-Y, Chen Y-H, Fan L-S, Kim H, Gao X, Ling T-C, Chiang P-C, Pei S, Gu G (2020): CO_2 mineralization and utilization by alkaline solid wastes for potential carbon reduction. Nature Sustainability Nature Sustainability, 1-7
10. Ćwik A, Casanova I, Rausis K, Koukouzas N, Zarębska K (2018): Carbonation of high-calcium fly ashes and its potential for carbon dioxide removal in coal fired power plants. Journal of Cleaner Production 202, 1026-1034
11. Ho HJ, Iizuka A, Shibata E (2021): Utilization of low-calcium fly ash via direct aqueous carbonation with a low-energy input: Determination of carbonation reaction and evaluation of the potential for CO(2) sequestration and utilization. J Environ Manage 288, 112411
12. Wang B, Pan Z, Cheng H, Guan Y, Zhang Z, Cheng F (2020): CO2 sequestration: high conversion of gypsum into CaCO3 by ultrasonic carbonation. Environmental Chemistry Letters 18, 1369-1377
13. Azdarpour A, Afkhami Karaei M, Hamidi H, Mohammadian E, Honarvar B (2018): CO2 sequestration through direct aqueous mineral carbonation of red gypsum. Petroleum 4, 398-407
14. Altiner M, Top S, Kaymakoğlu B, Seçkin İY, Vapur H (2019): Production of precipitated calcium carbonate particles from gypsum waste using venturi tubes as a carbonation zone. Journal of CO2 Utilization 29, 117-125
15. Li H, Tang Z, Li N, Cui L, Mao X-z (2020): Mechanism and process study on steel slag enhancement for CO2 capture by seawater. Applied Energy 276, 115515
16. Yuan Y, Lu W, Cheng W, Qi G, Hu X, Su H, Wang M, Zhang M, Liang Y (2022): Method for rapid mineralization of CO2 with carbide slag in the constant-pressure and continuous-feed way and its reaction heat. Powder Technology 398, 117148
17. Liu S, Liu W, Jiao F, Qin W, Yang C (2021): Production and resource utilization of flue gas desulfurized gypsum in China - A review. Environmental Pollution 288, 117799
18. Lee Mg, Jang YN, Ryu Kw, Kim W, Bang J-H (2012): Mineral carbonation of flue gas desulfurization gypsum for CO2 sequestration. Energy 47, 370-377
19. Wang B, Pan Z, Du Z, Cheng H, Cheng F (2019): Effect of impure components in flue

gas desulfurization (FGD) gypsum on the generation of polymorph CaCO3 during carbonation reaction. Journal of Hazardous Materials 369, 236-243

20. Ding W, Qiao J, Zeng L, Sun H, Peng T (2023): Desulfurization gypsum carbonation for CO2 sequestration by using recyclable ammonium salt. International Journal of Greenhouse Gas Control 123, 103843
21. Wang Y, Zheng X, Wang Y, He Q, Yan S, Ji L (2023): Amine-promoted gypsum carbonation for efficient CO2 capture and selective synthesis of CaCO3 polymorph integrating with amine regeneration by bipolar membrane electrodialysis. Chemical Engineering Journal 478, 147335
22. Pane I, Hansen W (2005): Investigation of blended cement hydration by isothermal calorimetry and thermal analysis. Cement and Concrete Research 35, 1155-1164
23. Ebrahimi A, Saffari M, Milani D, Montoya A, Valix M, Abbas A (2017): Sustainable transformation of fly ash industrial waste into a construction cement blend via CO2 carbonation. Journal of Cleaner Production 156, 660-669
24. Muljani S, Setyawan H, Nugraha RE (2023): Bubble formation phenomenon on the absorber column for CO2 absorption and to produce precipitated silica sodium carbonate. RSC Advances 13, 33471-33483
25. Xiangli N, Fenghua L, Enzhu H. CO_2 sequestration by red mud under coupling effect of ultrasonic wave and mechanical agitation. Chinese Journal of Environmental Engineering 12(10):2973-2979.
26. Jo HY, Ahn JH, Jo H (2012): Evaluation of the CO2 sequestration capacity for coal fly ash using a flow-through column reactor under ambient conditions. J Hazard Mater 241-242, 127-36
27. Zhao H, Li H, Bao W, Wang C, Li S, Lin W (2015): Experimental study of enhanced phosphogypsum carbonation with ammonia under increased CO2 pressure. Journal of CO2 Utilization 11, 10-19
28. Haghnegahdar MR, Hatamipour MS, Rahimi A (2011): Mathematical modeling of CO2 capture in a semi-dry spouted bed reactor. Separation and Purification Technology 80, 509-518
29. Lu SQ, Lan PQ, Wu SF (2016): Preparation of Nano-CaCO3 from Phosphogypsum by Gas–Liquid–Solid Reaction for CO2 Sorption. Industrial & Engineering Chemistry Research 55, 10172-10177
30. Librandi P, Costa G, Souza ACBd, Stendardo S, Luna AS, Baciocchi R (2017): Carbonation of Steel Slag: Testing of the Wet Route in a Pilot-scale Reactor. Energy Procedia 114, 5381-5392
31. Song K, Kim W, Bang J-H, Park S, Jeon CW (2015): Polymorphs of pure calcium carbonate prepared by the mineral carbonation of flue gas desulfurization gypsum. Materials & Design 83, 308-313